

**ECONOMIC GEOLOGY
RESEARCH UNIT**

University of the Witwatersrand
Johannesburg

**FORMATION OF BEDDING-PARALLEL, THRUST-HOSTED
GOLD DEPOSITS, SABIE-PILGRIM'S REST GOLDFIELD,
EASTERN TRANSVAAL: THE ROLE OF FLUID PRESSURE**

M. HARLEY and E.G. CHARLESWORTH

• **INFORMATION CIRCULAR No. 263**

UNIVERSITY OF THE WITWATERSRAND
JOHANNESBURG

**FORMATION OF BEDDING-PARALLEL, THRUST-FAULTED
GOLD DEPOSITS, SABIE-PILGRIM'S REST GOLDFIELD,
EASTERN TRANSVAAL: THE ROLE OF FLUID PRESSURE**

by

M. HARLEY¹, ² and E.G. CHARLESWORTH²
(¹ Geological Survey, Private Bag X112, Pretoria 0001

² Department of Geology, University of the Witwatersrand,
Private Bag 3, P.O. WITS 2050, South Africa)

**ECONOMIC GEOLOGY RESEARCH UNIT
INFORMATION CIRCULAR No. 263**

May, 1993

**FORMATION OF BEDDING-PARALLEL, THRUST-HOSTED GOLD DEPOSITS,
SABIE-PILGRIM'S REST GOLDFIELD, EASTERN TRANSVAAL:
THE ROLE OF FLUID PRESSURE**

ABSTRACT

Shallowly dipping, thrust-hosted gold veins occur within the lower Proterozoic Transvaal Sequence rocks in the eastern Transvaal of South Africa. Internally, the veins record numerous episodic events of fluid infiltration and mineral deposition within discrete local-scale thrust faults. Evidence exists for subvertical dilation increments within the individual veins and textures recording open-space filling are also preserved. The implied depth of formation dictates lithostatic pressures in excess of 2.2kb and the vein textures indicate numerous reactivation events of the individual thrust faults, which occur in a terrane characterised by very low levels of preserved strain. Friction theory arguments suggest that fault reactivation may occur under conditions of very low differential stress in the presence of high pressure fluids, with P_{fluid} approaching or exceeding lithostatic levels.

____oOo____

**FORMATION OF BEDDING-PARALLEL, THRUST-HOSTED GOLD DEPOSITS,
SABIE-PILGRIM'S REST GOLDFIELD, EASTERN TRANSVAAL:
THE ROLE OF FLUID PRESSURE**

CONTENTS

	Page
INTRODUCTION	1
GEOLOGICAL SETTING OF THE AURIFEROUS REEFS	1
REEF STRUCTURE	1
Stage 1	4
Stage 2	6
Stage 3	8
DISCUSSION	8
FLUID PRESSURE AND FAULTING	10
APPLICATION TO THE SABIE-PILGRIM'S REST GOLDFIELD	14
CONCLUSIONS	15
ACKNOWLEDGEMENTS	16
REFERENCES	16

____ oOo ____

Published by the Economic Geology Research Unit
Department of Geology
University of the Witwatersrand
1 Jan Smuts Avenue, Johannesburg 2001
South Africa

ISBN 1 86838 060 2

FORMATION OF BEDDING-PARALLEL, THRUST-HOSTED GOLD DEPOSITS, SABIE-PILGRIM'S REST GOLDFIELD, EASTERN TRANSVAAL: THE ROLE OF FLUID PRESSURE

INTRODUCTION

The Sabie-Pilgrim's Rest Goldfield is situated on the preserved, westerly dipping rim of the early Proterozoic Transvaal Basin, in the eastern Transvaal, South Africa (Fig.1). The Transvaal Sequence consists of a basal succession of arenaceous and argillaceous sedimentary rocks and volcanic lithologies confined to restricted proto-basins, comprising the Wolkberg (Button, 1973) and Godwan Groups (Myers, 1990). The protobasinal assemblages are overlain by the laterally extensive carbonate-siliciclastic sequence, comprising the Malmani Subgroup (Fig.2) (Button, 1986; Clendenin, 1989). The uppermost stratigraphic units of the Transvaal Sequence are represented by the alternating argillaceous and arenaceous lithologies of the Pretoria Group (Button, 1986; Eriksson and Clendenin, 1990). North-northeast-trending doleritic dykes are commonly developed within the Goldfield, as are pre- and syn-Bushveld Complex sills (Sharpe, 1984) of both doleritic and pyroxenitic compositions. Epigenetic gold mineralisation is hosted within a variety of rock types in the Sabie-Pilgrim's Rest Goldfield. The principal orebodies are stratiform, bedding-parallel, quartz-sulphide-gold vein deposits, locally termed "reefs". Transgressive leader veins and vertical reefs have also been mined. This paper describes the structure and environment of reef development and explores the role of fluid pressure in ore-deposit genesis within the Sabie-Pilgrim's Rest Goldfield.

GEOLOGICAL SETTING OF THE AURIFEROUS REEFS

The majority of the auriferous reefs occur within the dolomitic units of the Malmani Subgroup (Fig.2), commonly in close association with interlayered carbonaceous shale bands, or in some instances, associated with mafic sills. In other formations, there is an association between the reefs and contact zones between rocks of contrasting competency, *e.g.* sandstone and shale. A clearly defined mechanical control to the localisation of mineralisation exists (Visser and Verwoerd, 1960; Zietsman, 1967; Tyler, 1989; Harley and Charlesworth, 1991a). Flat reefs cannot be traced for more than 10km without interruption. Reefs may, however, be present at similar stratigraphic elevations, but at widely spaced localities within the Goldfield. Tyler (1989) suggested that there is a link between mineralisation and shale units deposited in what he considered to be supratidal environments. In contrast, Clendenin (1989) provided substantial evidence showing that all shale units are evidence of marine transgression, and record drowning of the basin and cessation of carbonate production. Ideas such as these have potential significance with respect to exploration, but in the context of this paper the origin of the host lithologies is not considered to be significant.

REEF STRUCTURE

Ten flat reef deposits were investigated in various degrees of detail, depending on available exposure. Most data for this publication has been derived from five well-exposed deposits (Nestor, Malieveld, Elandshoogte, Frankfort and Mountain Mines), with emphasis being placed on the Elandshoogte Reef, as exposed at the Elandshoogte Mine. This mine is

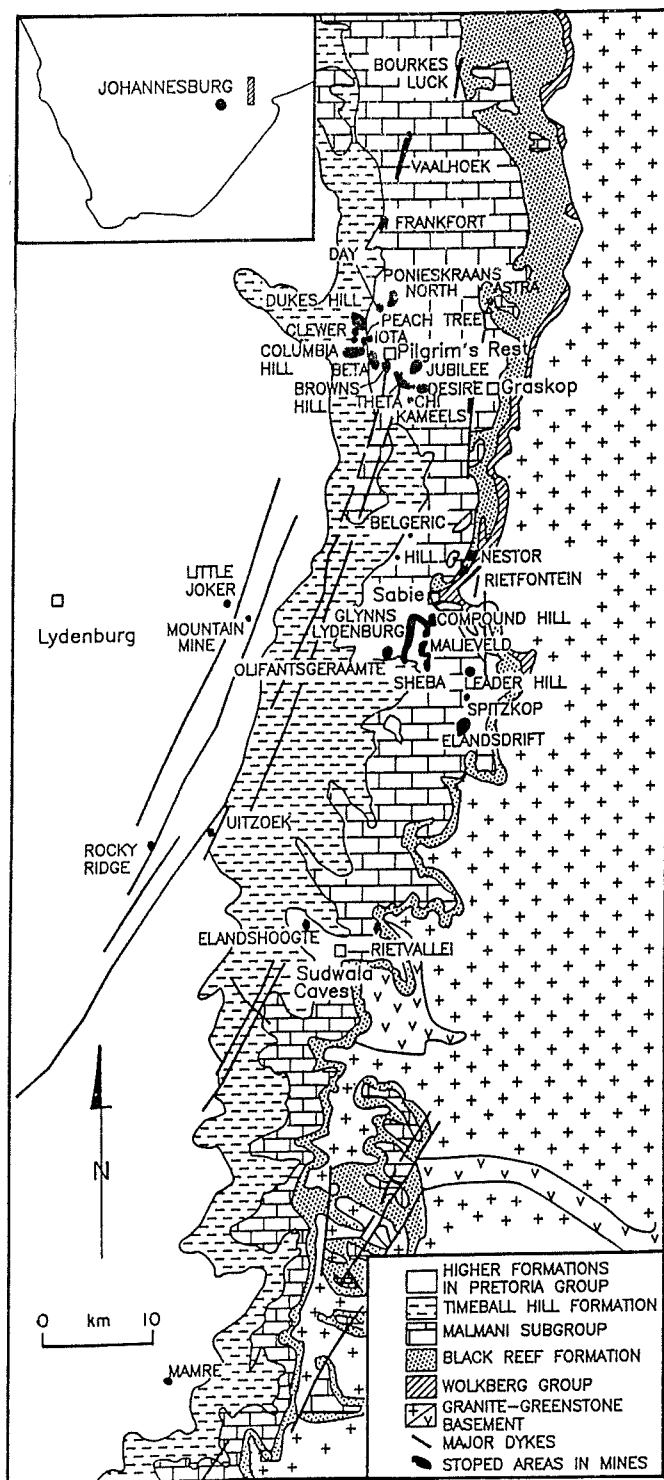


Figure 1: Geological map of the Sabie-Pilgrim's Rest Goldfield. The localities of the main gold deposits are indicated.

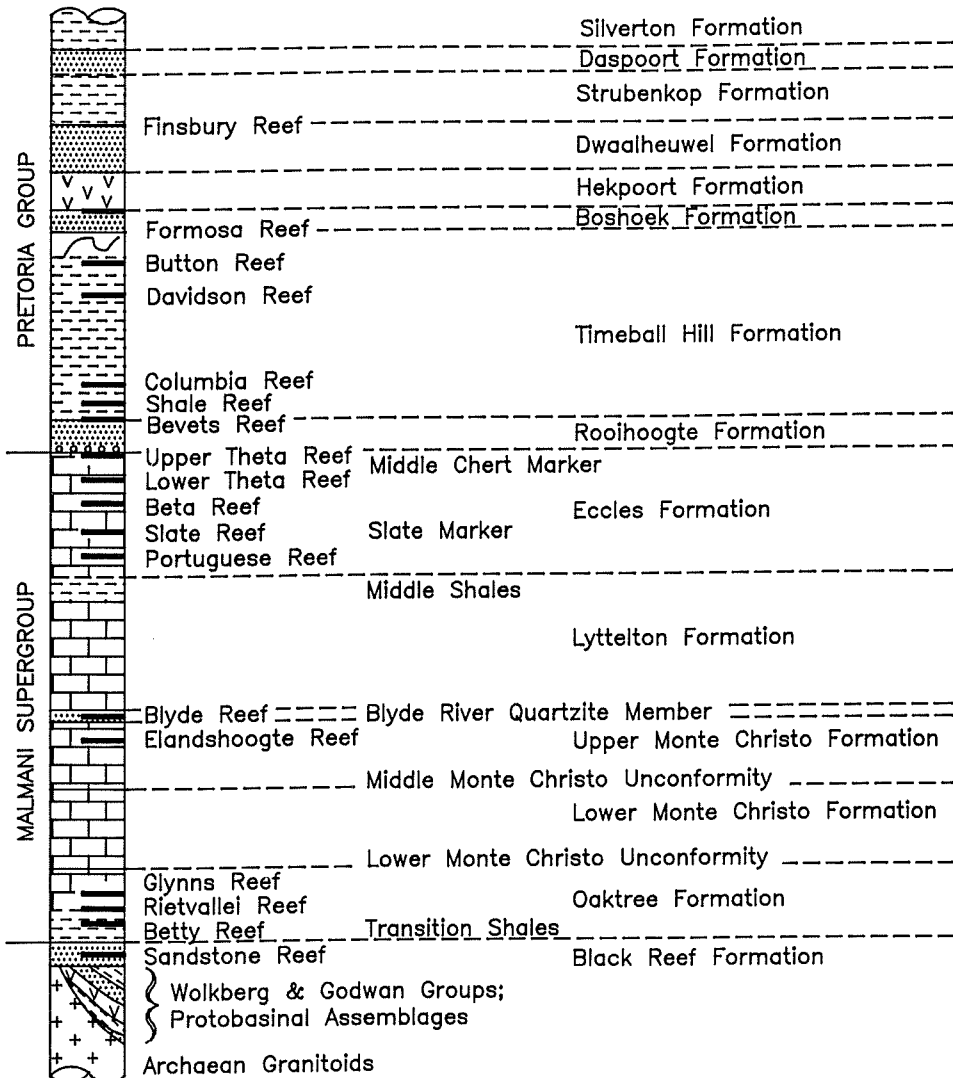


Figure 2: Stratigraphic column showing the lower Transvaal Sequence as developed in the Sabie-Pilgrim's Rest Goldfield. The positions of the main flat reefs are shown.

the only underground deposit currently being exploited (Fig.3) within the Goldfield. Extensive evidence of east to south-eastward directed bedding-parallel thrust-faulting in and around the flat reefs has been presented previously (Von Dessauer, 1912; Visser and Verwoerd, 1960; Zietsman, 1967; Tyler, 1989; Harley and Charlesworth, 1992). Evidence for similar deformation styles also exists in some weakly mineralised environments (Harley and Charlesworth, 1991b). There is evidence to show that flat reefs are oriented parallel to bedding. For example, at Elandshoogte Mine, the reef is seen, on a mine scale, to occur parallel to distinctive oolitic marker-beds. Typically, the dip of a flat reef lies between 4 and 7°, to the west, with some reefs dipping as steeply as 15°. Stopes maps of some mines suggest that there may be a preferred NNE elongation to the zone of economic mineralisation developed within a flat reef. However, in the mines around the village of Pilgrim's Rest, no distinct orientation can be recognised. Stopped areas on the flat reefs range from about 7000 by 200m in the case of Glynn's Lydenburg Mine (Fig.1) to the more typical dimension

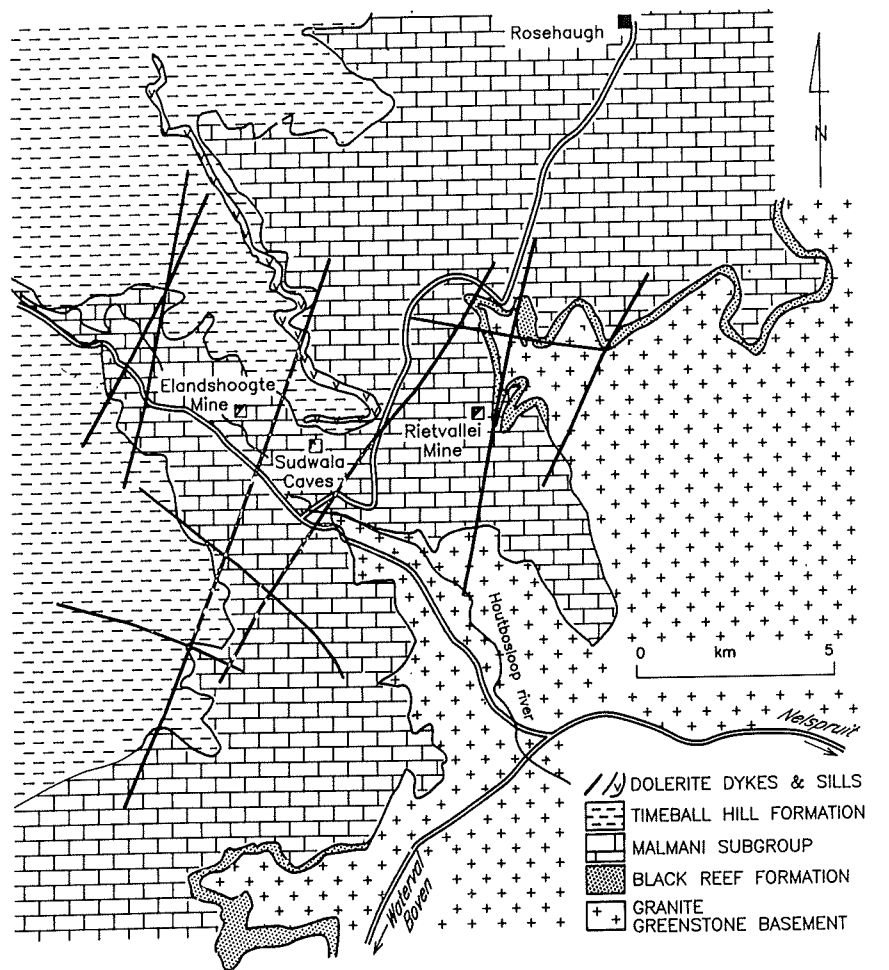


Figure 3: Detailed locality map of Elandshoogte Mine.

of 500 by 300m as recorded in the Elandshoogte Mine. The reefs rarely exceed 2m in thickness and are most commonly between 20 and 50 cm in thickness. In the case of Elandshoogte Reef (and others), the reef typically pinches and swells, both along strike and down dip. Computer-aided contouring of reef thickness, as determined during sampling procedures, reveals a randomly orientated set of saucer-shaped swells (>50cm thick), surrounded by pinched (>20 cm thick) zones. The internal structure of the Elandshoogte Reef is complex and several superimposed deformation and mineralisation events are recognised within this reef (Harley and Charlesworth, 1991a; 1992). The salient features of the events are described as follows:

STAGE 1

The earliest deformation is characterised by the formation of a subhorizontally orientated, close-spaced cleavage within the carbonaceous shale layer (Fig. 4) in which the reef is developed. The cleavage is defined by the subparallel alignment of fine-grained crystalline micas comprising the shale. Small euhedral pyrite cubes are present within the shale as isolated grains and cleavage-parallel laminae. The crystal faces of the pyrites cross-cut the cleavage planes within the shale, indicative that pyrite post-dates the formation of the



Figure 4: Detailed view of the Elandshoogte Reef showing the subhorizontal cleavage within the carbonaceous shale. Note also the occurrence of cleavage-parallel laminae of fine-grained pyrite within the shale and the coarse-grained pyrite within the massive quartz reef.

cleavage. Quartz-fibre pressure shadows are commonly developed around pyrite cubes within the shales, the individual fibres being oriented parallel to the cleavage planes in the shale. Coarser-grained, anhedral pyrite overgrows the earlier, fine-grained pyrites. Within the coarser pyrite, tightly folded trails of fine-grained pyrite are frequently preserved, marked by trails of carbonaceous inclusions within the coarse pyrite. Quartz-fibre-filled pressure shadows are uncommonly preserved around coarse-grained pyrite masses.

Three generations of coarse-grained pyrite are present. The first generation contains numerous inclusions of gangue material (it is this pyrite which displays the folding of pre-existing fine-grained pyrite layers) and is typically anhedral. Coarse-grained, inclusion-poor pyrite overgrows the pre-existing inclusion-rich pyrite. The inclusion-poor pyrite commonly displays well-developed cubic forms with moderately to strongly striated crystal faces. Round grains of gold, tennantite and chalcopyrite occur within the inclusion-poor, euhedral pyrite. Typically, the gold grains rarely exceed $10\mu\text{m}$ in dimension, whereas the host pyrite grain may exceed 20mm. Coarse-grained arsenopyrite occurs as subhedral, equant grains up to 1 cm in dimension, which are commonly intergrown with inclusion poor, euhedral pyrite.

Narrow selvages of inclusion-bearing pyrite occur as incomplete envelopes around the inclusion-poor pyrite. Frequently, these selvages have well-developed crystal faces. Within the first stage of mineralisation, evidence of deformation accompanying mineralisation is most evident in the crystal-matrix relationships between pyrite and shale, as have been described. Because later deformation events largely overprint these relationships, they can only be observed in certain areas of the mine, following extensive and detailed mapping of the development sidewalls. The formation of pressure-shadows is good evidence for simple-

shear deformation processes, supported by the development of asymmetric folds within the shales. The occurrence of small-scale folds (as described previously) overgrown by coarse-grained pyrite indicates broadly overlapping deformation and mineralisation. Identical styles of folding are developed within the shales. These tight, millimetre-scale folds are asymmetric and are developed above narrow décollement surfaces. Fold vergence is eastwards and axial planes strike between 350° and 030° and dip approximately 30° westwards.

STAGE 2

The second stage of reef development is marked by a profound change in the deformation and mineralisation style within the reefs. Whereas the deformation effects of Stage 1 occurred mainly as bedding-parallel shearing, with notable folding of the pre-existing cleavage within the shale, Stage 2 is dominated by the development of brittle fractures and the accompanying development of quartz veins.

During Stage 2 of reef development, the dolomite immediately over- and underlying the shale and reef package is totally replaced with microcrystalline quartz (frequently termed chert), for up to 1.2 m from the reef margins. The upper and lower contacts of the silicified zone with the surrounding dolomites are sharp and are frequently located along a well-developed bedding surface, particularly in the case of the contact between the silicified zone and the hanging-wall dolomite. The lower contact, between the silicified zone and the underlying, unaltered dolomite is generally undulose and frequently transgresses bedding at low angles. Disseminated pyrite is developed within the silicified zones, as is fine-grained muscovite. Quartz veins and, to a lesser extent, veins comprising quartz + carbonate, are present within the silicified zones. Two dominant orientations of vein are present: one set varies in dip from subhorizontal attitudes to shallow easterly dipping orientations, the second set dips steeply to the east (Fig. 5a). These veins may occur singly or as densely clustered arrays and frequently the two sets intersect. Detailed investigations of the vein intersections show no cross-cutting relationships and indicate that the veins were probably developed contemporaneously. Both vein orientations show stepped offsets. In any one exposure the sense of stepping of the steep veins is opposite to that of the shallowly dipping veins. Shallowly dipping veins step down to the east, steep veins step down to the west. The different senses of step of these veins is a function of their opening history; shallow-dipping veins have a "top to the east" opening history, whilst the steep-dipping veins have a "top to the west" opening history. Such observations are consistent with these two vein orientations being developed along riedel and conjugate riedel fractures respectively (Fig. 5b). The sense of shear associated with the formation of these two vein sets is compatible with that of an easterly verging bedding-parallel thrust system.

Laminated quartz veins, with inclusions of pre-existing pyrite, occur parallel to the subhorizontal cleavage in the shale (Figs. 6 and 7). Septa of carbonaceous wall-rock separate the vein strands, some of which are folded. The individual laminated, or ribboned veins are seldom thicker than 2 cm and most veins cannot be traced for more than 2m. The ribboned veins taper sharply closed at their tips and do not display branches. Rather they maintain their thickness for most of their length.

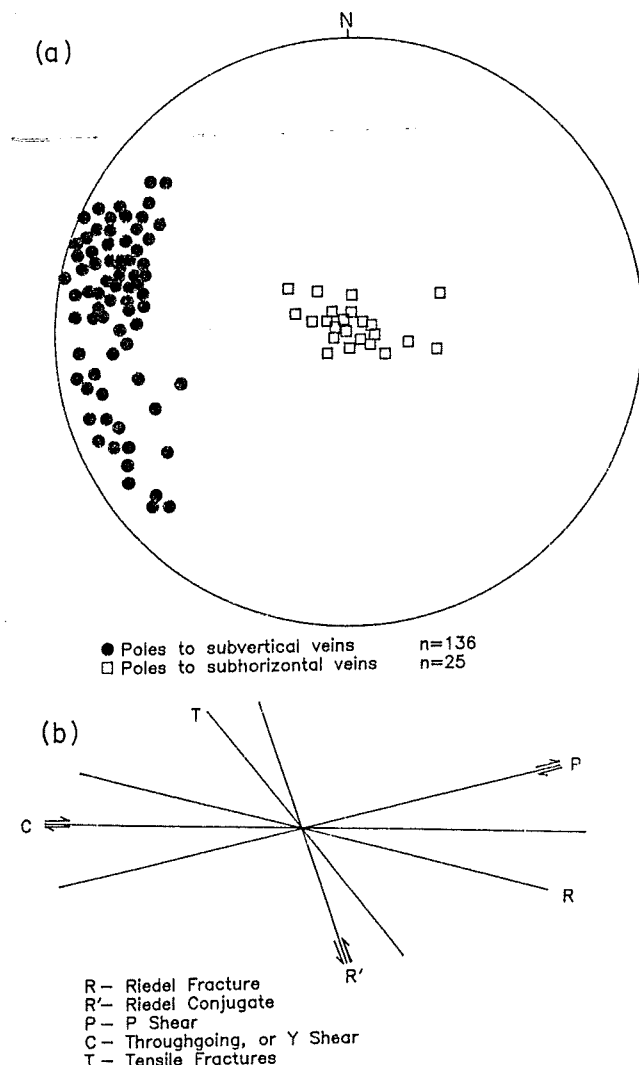


Figure 5(a). Lower hemisphere, equal area projection showing the orientation of shallowly dipping and steeply dipping veins surrounding the Elandshoogte Reef.

*(b) Schematic profile view showing the elements of a brittle shear fracture array.
Overall sense of shear is dextral.*

The ribboned or laminated veins are commonly preserved along the margins of the reef. The centre of the quartz-sulphide reef is occupied by a massive quartz vein, which locally truncates the ribboned segments along its periphery (Fig. 6). Internally, the massive quartz vein displays a complex structure and many features deserve description. The vein consists of anhedral buck quartz, in which fragments of silicified dolomite, pre-existing sulphides and fragments of wall-rock septa are preserved. Locally, the fragments of silicified dolomite are abundant enough to constitute breccias. Two types of breccia can be distinguished on a textural basis, namely, chaotic and mosaic breccias. Chaotic breccias (Fig. 7) consist of numerous small clasts of silicified dolomite set in massive quartz. Clasts are randomly arranged, but tend to be fairly equant in form. Packing of the clasts within the reef quartz is highly variable and ranges from sparse to dense in concentration.

Mosaic breccias contain large-to-small, fragments of silicified dolomite often with complex shapes (Fig. 8). These breccias are formed by disaggregation of silicified dolomite and dilation. Clasts are rarely in contact, and are almost invariably surrounded by quartz vein material. In a mosaic breccia, fragments are invariably angular and all preserve sharp corners. There is no evidence of preferential dissolution at apices of clasts. Chaotic breccias frequently occur as discontinuous podiform bodies within the reef, which are rarely developed for more than 5m along strike or down dip. Mosaic breccias are developed as discontinuous offshoots from the reef, most commonly within the silicified dolomite immediately overlying the reef, or are developed within the reef itself. In the latter case, relatively "clean" reef grades laterally into a mosaic breccia vein, which may extend for more than 50 m along strike or down dip.

Small vugs lined with concentric layers of euhedral quartz crystals are commonly present in many reef units (e.g. Harley and Charlesworth, 1991a; M. Meyer pers. comm. 1993) and are good evidence supportive of open space filling (Fig. 9). Pyrite and arsenopyrite masses occur as inclusions within the massive quartz and also within the breccia environments. The sulphides are cataastically fractured and laced with a network of fine fractures filled with quartz, which is in optic continuity with the enclosing massive quartz. Coarse-grained muscovite also occurs within the massive quartz, and in some cases muscovite is present in the microveinlets within the fractured sulphide minerals. A suite of rare minerals accompanies deposition of the later, more massive vein quartz. These include native bismuth and bismuthinite, gold, fahlores (typically tennantite in the case of Elandshoogte) and chalcopyrite, which is volumetrically dominant. In many cases, the late-stage minerals occur within microveinlets within the fractured pyrite, and do not obviously replace the surrounding pyrite, with the notable exception of gold. Gold may occur as discrete grains within the fractures, or may be observed in direct contact with one or more of the other late-stage minerals, but always replaces pyrite.

STAGE 3

The final stage of reef development is one in which the reef undergoes deformation as a blind thrust system (Harley and Charlesworth, 1991a). The footwall and hanging-wall thrusts to this system are located at or close to the upper and lower contacts of the reef (Figs. 10 and 11). Fault strands transgress the reef from the footwall to the hanging-wall and duplex arrays are commonly developed consisting of interlayered slices of quartz and shaly material (Fig. 10). Antiformal stacks and locally developed backthrust structures (Fig. 11) are also commonly recognised. No mineralisation accompanies this deformation event which verges to the east-southeast.

DISCUSSION

Textural evidence, from subhorizontal and steeply inclined veins within the silicified zones, indicates that these veins formed together. The orientation of the steeply inclined veins is consistent with that of the riedel conjugate (R'), whilst the subhorizontal veins occupy the riedel and P shears of a brittle shear system (Fig. 5b). The passive rotation of these fractures during prolonged or continuous deformation led to their dilation, and subsequent infilling by quartz. It is possible to describe the state of stress responsible for

Figure 6: Laminated or ribboned quartz veins, well developed along the Reef hanging-wall contact, Elandshoogte Mine.

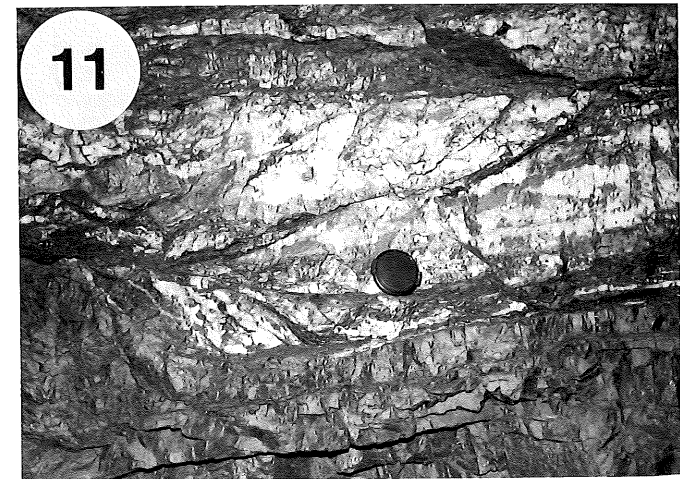
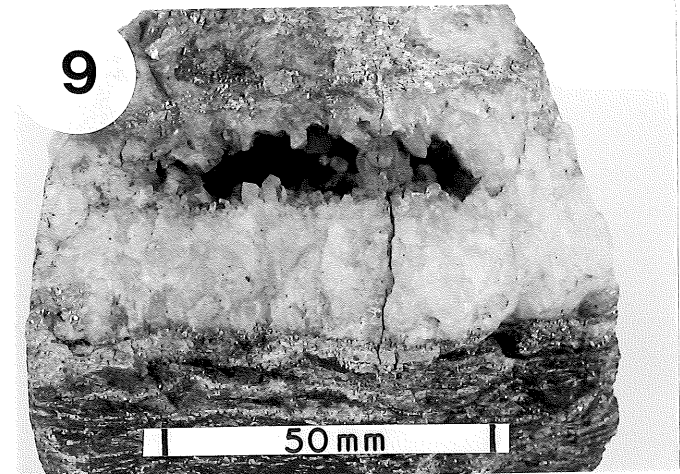
Figure 7: Quartz ribbon veins interlayered within well-mineralised shale adjacent to lens-cap. Note the development of chaotic breccia (consisting of shale and silicified dolomite fragments within reef quartz) present beneath the shale.

Figure 8: Mosaic breccia developed within the Elandshoogte Reef, consisting of angular, silicified dolomite fragments, surrounded by reef quartz and pyrite.

Figure 9: Hand specimen from the Bevets Reef, Frankfort Mine, showing the development of euhedral quartz crystals within a small vug present in the reef. Note also the presence of fine-grained pyrite laminae within the carbonaceous shale at the base of the sample.

Figure 10: Duplex array consisting of horses of reef quartz, Elandshoogte Mine. These deformation features, developed in Stage 3 (see text) are confined to the reef and its immediate vicinity, forming a blind thrust system.

Figure 11: Complex deformation within the Elandshoogte Reef. One duplex array, developed beneath the lens-cap, verges to the left of the photograph whilst the larger array, above the lens-cap, verges to the right. The former array preserves evidence of limited backthrust deformation.



deformation in terms of three *compressive stress axes*. The σ_2 (intermediate stress) axis of the stress ellipsoid, consistent with the observed deformation is subhorizontal and trends north-northeast, parallel to the line of intersection between the riedel and the conjugate riedel fractures (Fig. 5a and b). This situation is also consistent with the orientation of fold-forms within deformed shales associated with the reef. Ideally, σ_1 should bisect the acute angle between the riedel and the riedel conjugate fractures (*e.g.* Hodgson, 1989). However, in reality, it may also be inclined at any acute angle to the riedel fractures (Hodgson, 1989). In the case of the Sabie-Pilgrim's Rest Goldfield, considering the environment in which these thrust faults are developed (shallow-dipping, laterally extensive sheets of sedimentary rocks) it is assumed that σ_1 lies subhorizontal and trends east-southeast to west-northwestwards. On a regional scale, within the Goldfield strain, is heterogeneously distributed. Effects of high strain are restricted to the immediate vicinity (within 1m) of the reefs. In contrast, strain in unmineralised areas is extremely low, with the noted absence of fold and cleavage formation.

FLUID PRESSURE AND FAULTING

An important feature of the mineralisation and deformation style of the Elandshoogte Reef is the episodic nature of the mineralisation, arising from repeated reactivation of the low-angle, bedding-parallel thrust fault which hosts mineralisation. Mineral deposition occurred as successive, repeated episodes within the reef. These mineralisation events closely overlapped in time with a progressive deformation sequence, which commenced with shearing within the incompetent shales and finished with duplex thrusting within the competent reef band. Identical reef development histories have been established for the five well-exposed deposits investigated during this study (Harley, 1993).

The observed reactivation of the low-angle thrusts has important implications for the role of fluid pressure during mineralisation and deformation. Subhorizontal vein components are commonly developed in the reef with ribboned vein textures recording incremental opening, and crystal-lined vugs indicating episodic open-space filling. These observations imply that extension was parallel to the subvertical axis, subparallel to the minimum compressive stress, σ_3 , and provides strong evidence in support of high (supralithostatic) fluid pressures during vein growth. The influence of fluid pressure on faulting in general, has been the subject of recent work (Sibson, 1981, 1985, 1989; Sibson *et al.*, 1988; Reynolds and Lister, 1987; Cox, 1991; Cox *et al.*, 1991, among others) and the approaches used by these authors have been applied to the Sabie-Pilgrim's Rest Goldfield in this study. The frictional strength of an existing fault may be approximated by a Coulomb-type criterion (Sibson, 1985) as follows:

$$\tau = C + \mu \sigma_n' \quad \text{or} \quad \tau = C + \mu(\sigma_n - P_f) \quad (1)$$

where μ is the coefficient of static friction, σ_n is the normal stress across the fault,

τ is the shear stress across the fault, C is the cohesive strength of the fault and

P_f is the fluid pressure.

The effective normal stress, $\sigma_n' = \sigma_n - P_f$ (Hubbert and Rubey, 1959).

Taking the simplest case of a cohesionless fault and allowing $C = 0$ the expression simplifies to:

$$\tau = \mu(\sigma_n - P_f) \quad [2]$$

This equation can be expressed in terms of the acting effective stresses, written in the nomenclature of the Mohr stress circle (Ramsay and Huber, 1987, Appendix E), where θ is the angle between the fault and the maximum compressive stress axis, σ_1 .

The effective shear stress, $\tau' = \tau = (\sigma'_1 - \sigma'_3) \sin 2\theta / 2$ and the effective normal stress, σ'_n can be written as

$$\sigma'_n = \sigma_n - P_f = (\sigma'_1 + \sigma'_3) / 2 - (\sigma'_1 - \sigma'_3) \cos 2\theta / 2 \quad [4]$$

Substitution of these fundamental equations 3 & 4, into equation 2 gives:

$$(\sigma'_1 - \sigma'_3) \sin 2\theta = \mu \{(\sigma'_1 + \sigma'_3) - (\sigma'_1 - \sigma'_3) \cos 2\theta\}$$

which expands to give:

$$\sigma'_1 \{\sin 2\theta + \mu(\cos 2\theta - 1)\} = \sigma'_3 \{\sin 2\theta + \mu(\cos 2\theta + 1)\}$$

Now, if we define $R = \sigma'_1 / \sigma'_3$ (Sibson, 1985)
then $R = \{\sin 2\theta + \mu(\cos 2\theta + 1)\} / \{\sin 2\theta + \mu(\cos 2\theta - 1)\}$
which gives:

$$R = (1 + \mu \cot \theta) / (1 - \mu \tan \theta) \quad [6]$$

Since $R = \sigma'_1 / \sigma'_3 = (1 + \mu \cot \theta) / (1 - \mu \tan \theta)$, it is possible to calculate the absolute differential stress, $(\sigma_1 - \sigma_3)$ (Sibson, 1989), required for reactivation faulting under a set of predetermined conditions. The equation defining the differential stress is:

$$(\sigma_1 - \sigma_3) = \mu \{(\tan \theta + \cot \theta) / (1 - \mu \tan \theta)\} \sigma'_3 \quad (\text{Sibson, 1989}). \quad [7]$$

But the effective minimum stress, $\sigma'_3 = (\sigma_3 - P_f)$ where P_f is the fluid pressure.
Expanding the expression: $\sigma'_3 = \rho g z (1 - \lambda)$, where ρ is the depth-integrated rock density, z is the depth to the point of failure, and λ is the ratio of fluid pressure P_f to lithostatic pressure, i.e. $\lambda = P_f / \rho g z$

For a stress field in which σ_3 is vertical (or approximately so), equation [7] may be expanded (Sibson, 1989) to give:

$$(\sigma_1 - \sigma_3) = \mu \{(\tan \theta + \cot \theta) / (1 - \mu \tan \theta)\} \{\rho g z (1 - \lambda)\} \quad [8]$$

The ratio R approaches infinity as θ (the angle θ is termed the reactivation angle; Sibson, 1985) approaches zero.

The reefs or faults of the Sabie-Pilgrim's Rest Goldfield are typically inclined at 3-10°. Assuming a near field stress σ_1 , which is approximately subhorizontal (as suggested by

orientations of riedel and conjugate riedel fractures, and the overall shear sense indicators), a value of 5° is adopted as a best estimate for the reactivation angle, implying $R \approx 18$. In other words, $\sigma_1'/\sigma_3' \approx 18$, showing that $\sigma_1' > > \sigma_3'$. However, no recognised cleavage has been described from the dolomites surrounding the reef (or the dolomites in the Eastern Transvaal in general). Moreover, the predominant stylolite direction is subhorizontal and large-scale folding of unmineralised rock is absent in the Sabie-Pilgrim's Rest Goldfield, indicating low levels of preserved strain in the dolomites with absolute values for σ_1' and σ_3' too low to result in widespread deformation.

A further condition for reactivation of low (and also high) angle faults is that σ_3' must approach 0. Or, as otherwise stated, $\sigma_3 \rightarrow P_f$ (Sibson, 1985). Thus the magnitude of fluid pressure must approach the lithostatic pressure. It follows that as $\sigma_3' \rightarrow 0$, so $R \rightarrow \infty$ and it becomes less possible to define the shape of the stress ellipsoid. The high fluid pressure condition suggested here is confirmed in the following analysis considering the fields of intact shear failure and reactivation faulting.

The influence and importance of fluid pressure on reactivation faulting is clearly illustrated when the case of reactivation versus intact rock failure is considered. Hubbert and Rubey (1959), in a mathematical analysis of overthrust faulting, demonstrated that in the absence of a "lubricating layer" to reduce frictional resistance, overthrust faulting (low-angle thrusting) was not possible because intact shear failure of the overthrust block would be expected to occur, with the development of steeper "Andersonian" faults cutting through the overlying block before low angle thrusting was initiated. The Coulomb criterion which expresses the conditions of shear failure for compressed material has been previously introduced.

$\tau = C + \mu\sigma_n' = C + \mu(\sigma_n - P)$, this may be rewritten in terms of the effective principal stresses as

$\sigma_1' = \sigma_0 + K\sigma_3'$ (Sibson, 1989); where $K = [(1 + \mu^2)^{1/2} + \mu]^2$ and σ_0 is the uniaxial compressive strength of the rock under consideration.

Recasting this expression to define differential stress (Sibson, 1989) gives:

$$(\sigma_1 - \sigma_3) = \sigma_0 + (K - 1)\sigma_3' \quad [9]$$

Now, allowing the conditions under which intact shear failure occurs to equal those characterised by reactivation fault failure (i.e. equating Equations [8] and [9]), the position of the boundary separating the fields of intact shear failure versus reactivation fault failure may be calculated.

$$\mu[(\tan\theta + \cot\theta)/(1 - \mu\tan\theta)]\sigma_3' = \sigma_0 + (K - 1)\sigma_3'$$

$$\mu[(\tan\theta + \cot\theta)/(1 - \mu\tan\theta)] = (\sigma_0/\sigma_3') + (K - 1)$$

$$\mu[(\tan\theta + \cot\theta)/(1 - \mu\tan\theta)] - K + 1 = \sigma_0/(\rho g z (1 - \lambda))$$

$$\sigma_0/\rho g z \{ \mu [(\tan\theta + \cot\theta)/(1 - \mu \tan\theta)] - K + 1 \} = 1 - \lambda \quad [10]$$

It is possible to solve for the boundary position, in terms of λ and θ (the reactivation angle), under conditions of preset depth, density, etc applicable to the Sabie-Pilgrim's Rest Goldfield.

Figure 12 shows the intact shear field and the field of reactivated shear under conditions applicable to the Sabie-Pilgrim's Rest Goldfield. The value of σ_0 , the compressive axial strength of dolomite, in the case of many reefs of the Sabie-Pilgrim's Rest Goldfield is derived from compiled strength values for carbonate rocks quoted by Brink (1979) and Jaeger and Cook (1979). Reactivation faulting may only occur at a reactivation angle of 5°, given high fluid pressures, equal to or exceeding lithostatic pressure. This analysis assumes the cohesive strength, $C=0$. Sibson (1981) demonstrated that hydrofracture is not possible for cohesionless faults, and the necessary inclusion of a term approximating C requires that this additional strength be overcome by P_f , i.e. P_f must exceed lithostatic pressures (Sibson, 1985; Sibson *et al.*, 1988). It is possible to reactivate a fault, for which the R value is high, with a low absolute σ'_1 value (*i.e.* low differential stress) when σ_3' approaches 0, (*i.e.* $\sigma_3=P_f$).

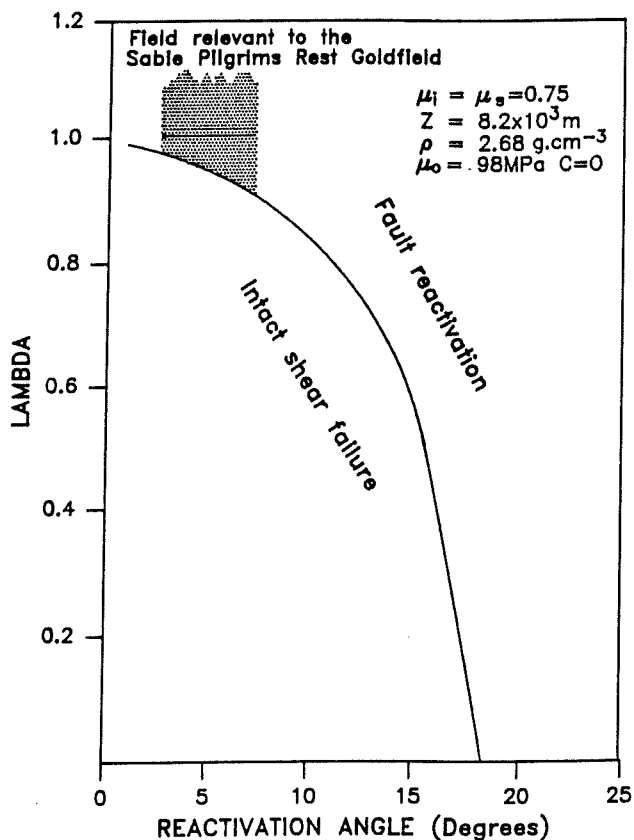


Figure 12: Graph of lambda (λ) versus reactivation angle (θ) for bedding-parallel, thrust-hosted gold veins of the Sabie-Pilgrim's Rest Goldfield. The fields of reactivation and intact shear failure are indicated.

The expression evaluating the differential stress required for fault reactivation, for different values of the reactivation angle θ , under any defined conditions of depth, density, coefficient of internal friction and λ has been derived previously (Equation [8]). Figure 13 is a plot of differential stress versus reactivation angle at conditions typical of the Sabie-Pilgrim's Rest Goldfield. The analysis breaks down at the limiting value of $1=\lambda$. It is, However, instructive to remember that derived values of differential stresses are minima because of the exclusion of a term describing cohesive strength. Figure 13 suggests that a very low differential stress would be required to reactivate the shallow-dipping thrusts, provided $\lambda \approx 1$.

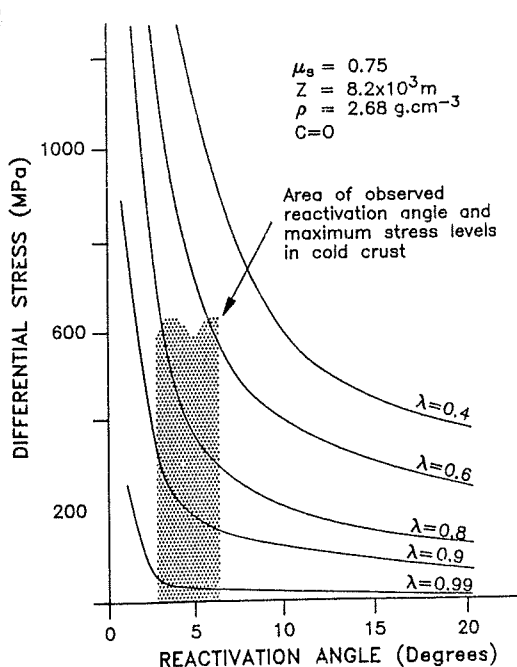


Figure 13: Graph of differential stress ($\sigma_1 - \sigma_3$) versus reactivation angle (θ) for bedding-parallel, thrust-hosted gold veins of the Sabie-Pilgrim's Rest Goldfield. Curves for various values of lambda (λ) are plotted.

APPLICATION TO THE SABIE-PILGRIM'S REST GOLDFIELD

Assuming that the vein mineralisation in the Sabie-Pilgrim's Rest Goldfield is syn-Bushveld in age (Boer *et al.*, 1993), the depth to the auriferous reefs at the time of mineralisation is the cumulative height of the overlying Transvaal Sequence stratigraphy up to the base of the Bushveld Complex, corrected for major regional thickness variations. The stratigraphic thickness for the upper Transvaal Sequence in the eastern Transvaal is approximately 8000m (Button, 1973; 1986), indicating a lithostatic pressure of approximately 2.2-2.5 kb at typical depths of reef formation in the Pilgrim's Rest area and, possibly slightly more in the Sabie area. With such low reactivation angles, as encountered in the Sabie-Pilgrim's Rest Goldfield, reactivation faulting will only take place, under low levels of differential stress, with high values of λ (Figs. 12 and 13). Under calculated conditions applicable to the Goldfield, reactivation faulting may occur at differential stresses less than 20MPa, dependent upon the accepted cohesion across the fault. Byerlee (1978) has shown

that alteration minerals, such as muscovite, which typically occurs in fault gouges, does not significantly affect the frictional resistance across the fault surface. Minerals such as montmorillonite and vermiculite however, may reduce frictional drag. In the light of this, a value of $\mu_0 = 0.75$ is adopted for the typical fault plane, consistent with quoted values of friction, by Byerlee (1978) and Sibson (1989). These observations are all consistent with the observed low levels of strain in the eastern Transvaal and have implications for the valve behaviour of the reef (Sibson, 1991), namely that fluid pressure variations will have a major effect in controlling fault motion within the reef environment, rather than differential stress variations.

Fluid pressure must, of necessity, also be high to permit the post-reef thrust deformation of the reef to occur. Secondary trails of low-salinity fluid inclusions have been observed cross-cutting the vein quartz of the reef. These inclusions post-date the mineralisation of the reef and are interpreted to represent fracture planes and trapped fluids accompanying the post-reef thrust faulting described previously. The occurrence of orthogonal arrays of secondary inclusions sub-parallel and sub-perpendicular to the reef margins, (observed in the Elandshoogte Reef), have also been described from other quartz-vein deposits (Boullier and Robert, 1992). These inclusion trails are interpreted to represent *mode 1* tensional microcracks which occur perpendicular to σ_3 , following experimental (Brace and Bombolakis, 1963; Krantz, 1983), and field based (Pêcher *et al.*, 1985; Boullier and Robert, 1992) studies. The orthogonal orientations of these cracks indicate periodic switching of σ_3 from a subvertical to a subhorizontal orientation, probably in response to dynamic overshoot (Cox, 1991) following fault failure with an accompanying transient flip in the orientation of the near field stress regime.

The results of frictional analysis plotted on the two graphs (Figs. 12 and 13) indicate the following:

1. reactivation faulting of a low angle fault is not possible without transient high fluid pressures; λ must equal, or exceed unity for deformation to occur;
2. the differential stress in the Sabie-Pilgrim's Rest Goldfield, at the time of mineralisation, was not high enough to result in shear failure of intact dry rock, and in the absence of significantly high fluid pressures, no deformation would occur and no flat-reef style mineralisation would be possible.

The implications of this conclusion are that regional-scale localisation of mineralisation is probably a function of position of fluid source, rather than being directly related to any structural feature(s) present in the Transvaal Sequence rocks. The influence of structure on local and mine-scale mineralisation, however, is more significant.

CONCLUSIONS

The bedding-parallel gold reef deposits of the Sabie-Pilgrim's Rest Goldfield are hosted within shallowly dipping thrust faults of largely local extent. The observed styles of mineralisation and internal structures within the reefs indicate the influence of high fluid pressures. The structural setting of these reefs is also strongly supportive of high fluid pressures, equalling or exceeding lithostatic levels. The role of fluid pressure in the genesis

of gold veins in the Sabie-Pilgrim's Rest Goldfield was largely twofold; firstly, fluid pressure allowed faulting to occur under very low strain, generating permeability and creating and maintaining fluid pathways, secondly, fluid pressure was responsible for the maintenance of dilatancy. At depths below about 2km dilatancy, unsupported by fluid pressure, cannot be maintained (Fyfe *et al.*, 1978); the bedding-parallel veins of the Sabie-Pilgrim's Rest Goldfield can thus be likened to "water-sills" (Price, 1975; Fyfe *et al.*, 1978; Henderson *et al.*, 1990; Cox *et al.*, 1991), trapped within impermeable layers.

The source of the fluids is suggested to be extrabasinal, since related styles of gold mineralisation are also developed as vertical reefs within the granitoid basement beneath the Transvaal Sequence lithologies. If this is correct, the high fluid pressures are a direct consequence of their source environment, and it is not necessary to invoke mechanisms to account for generation of high fluid pressures within the Transvaal Sequence stratigraphy. Acceptance of a deep-seated magmatic source (possibly *related* to the Bushveld Complex) for the auriferous fluids (Boer *et al.*, 1993) can account for the inferred high fluid pressures and also has implications for mineral exploration. Flat reef deposits tend to occur in clusters centred around Sabie, Mount Anderson, Pilgrim's Rest and Bourkes Luck, with some deposits randomly scattered in between. It may be the case that the observed clustering of deposits reflects the positions of deep-seated intrusions. Therefore, areas peripheral to existing ore-deposit clusters may be more prospective than the areas between discrete clusters.

ACKNOWLEDGEMENTS

This work represents part of a Ph.D. thesis by the senior author, at the University of the Witwatersrand, and is published with permission of the Chief Director of the Geological Survey of South Africa. The authors thank Process and Mining Consultants and Makonjwaan Imperial Mining Company for access to deposits in the eastern Transvaal. Rudy Boer and Michael Meyer willingly engaged in discussions that have improved this paper. Lyn Whitfield, Di du Toit and Mark Hudson gave invaluable assistance with figure preparation and Janet Long prepared the final text.

REFERENCES

- Boullier, A-M. and Robert, F., 1992. Palaeoseismic events recorded in Archaean gold-quartz vein networks, Val d'Or, Abitibi, Quebec, Canada. *J. Struct. Geol.*, **14**: 161-179.
- Brace, W.F. and Bombolakis, E.G., 1963. A note on brittle crack growth in compression. *J. geophys. Res.*, **68**: 3709-3713.
- Brink, A.B.A., 1979. Engineering Geology of Southern Africa, Volume I. Building Publications, Pretoria, 319pp.
- Button, A., 1973. A regional study of the stratigraphy and development of the Transvaal Basin in the eastern and northern Transvaal. Unpublished Ph.D. thesis, Univ. Witwatersrand, Johannesburg, 352pp.

- Button, A., 1986. The Transvaal sub-basin of the Transvaal Sequence. In: Anhaeusser, C.R. and Maske, S. (Editors), Mineral Deposits of Southern Africa. Geological Society of South Africa, Johannesburg: Volume 1, 811-817.
- Byerlee, J.D., 1978. Friction of Rocks. Pure and Applied Geophysics, **116**: 615-626.
- Boer, R.H., Meyer, F.M., Robb, L.J., Graney, J.R. and Vennemann, T.W., 1993. The nature of gold mineralisation in the Sabie-Pilgrim's Rest Goldfield, eastern Transvaal, South Africa. Inform. Circ. Econ. Geol. Res. Unit, Univ. Witwatersrand, Johannesburg, 262 (In press).
- Clendenin, C.W., 1989. Tectonic Influence on the evolution of the early Proterozoic Transvaal sea, southern Africa. Unpublished Ph.D. thesis, Univ. Witwatersrand, Johannesburg, 367pp.
- Cox, S.F., 1991. Geometry and internal structures of mesothermal vein systems: implications for hydrodynamics and ore genesis during deformation. In: Structural Geology in Mining and Exploration. Geology Department and University Extension, University of Western Australia, Publ., **25**: 47-53.
- Cox, S.F., Wall, V.J., Etheridge, M.A. and Potter, T.F., 1991. Deformational and metamorphic processes in the formation of mesothermal vein-hosted gold deposits - examples from the Lachlan Fold Belt in central Victoria. Ore Geology Reviews, **6**: 391-423.
- Eriksson, P.G. and Clendenin, C.W., 1990. A review of the Transvaal Sequence, South Africa. J. Afr. Earth Sci., **10**: 101-116.
- Fyfe, W.S., Price, N.J. and Thompson, A.B., 1978. Fluids in the Earth's Crust. Elsevier, Amsterdam, 383pp.
- Harley, M., 1993. The geology of the Sabie-Pilgrim's Rest Goldfield with special reference to Elandshoogte Mine. Unpubl. Ph.D. thesis, Univ. Witwatersrand, Johannesburg, 275pp.
- Harley, M. and Charlesworth, E.G., 1991a. The mineralisation and structure of the Elandshoogte gold mine, Sabie-Pilgrim's Rest Goldfield, eastern Transvaal, South Africa. In: Ladeira, E.A.(Editor), Brazil Gold '91, The Economics, Geology, Geochemistry and Genesis of Gold Deposits. Balkema, Rotterdam: 685-692.
- Harley, M. and Charlesworth, E.G., 1991b. Compressive deformation in a pre-Bushveld sill, Sudwala, eastern Transvaal. S. Afr. J. Geol., **94**: 348-354.
- Harley, M. and Charlesworth, E.G., 1992. Thrust-controlled gold mineralisation at the Elandshoogte Mine, Sabie-Pilgrim's Rest Goldfield, South Africa. Mineralium Deposita **27**: 122-128.

- Henderson, J.R., Henderson, M.N. and Wright, T.O., 1990. Water-sill hypothesis for the origin of certain veins in the Meguma Group, Nova Scotia, Canada. *Geology*, **18**: 654-657.
- Hodgson, C.J., 1989. The structure of shear-related, vein-type gold deposits: a review. *Ore Geology Reviews*, **4**: 231-273.
- Hubbert, M.K. and Rubey, W.W., 1959. Role of fluid pressure in mechanics of overthrust faulting. *Bull. Geol. Soc. Amer.*, **70**: 115-166.
- Jaeger, J.C. and Cook, N.G.W., 1979. *Fundamentals of Rock Mechanics*. Chapman and Hall, London, 395pp.
- Kranz, R.L., 1983. Microcracks in rocks: a review. *Tectonophysics*, **100**: 449-480.
- Myers, R.E., 1990. The geology of the Godwan Basin, eastern Transvaal. Unpublished Ph.D. Thesis, Univ. Witwatersrand, Johannesburg, Vol 1 and 2: 320pp and 288pp.
- Pêcher, A., Lespinasse, M. and Leroy, J., 1985. Relations between fluid inclusion trails and regional stress field: a tool for fluid chronology - An example of an intragranitic uranium ore deposit (northwest Massif Central, France). *Lithos*, **18**: 229-237.
- Price, N.J., 1975. Fluids in the crust of the earth. *Sci. Progr. Oxf.*, **62**: 59-87.
- Ramsay, J.G. and Huber, M.I., 1987. *The Techniques of Modern Structural Geology, Volume 2: Folds and Fractures*. Academic Press, London, 700pp.
- Reynolds, S.J. and Lister, G.S., 1987. Structural aspects of fluid-rock interactions in detachment zones. *Geology*, **15**: 362-366.
- Sharpe, M.R., 1984. Petrography, classification and chronology of mafic sill intrusions beneath the Eastern Bushveld Complex. *Bull. Geol. Surv. S.A.*, **77**: 40pp.
- Sibson, R.H., 1981. Controls on low-stress hydro-fracture dilatancy in thrust, wrench and normal fault terrains. *Nature*, **289**: 665-667.
- Sibson, R.H., 1985. A note on fault reactivation. *J. Struct. Geol.*, **7**: 751-754.
- Sibson, R.H., 1989. High-angle reverse faulting in northern New Brunswick, Canada, and its implications for fluid pressure levels. *J. Struct. Geol.*, **11**: 873-877.
- Sibson, R.H., 1991. Fluid flow in seismogenic crust. In: *Structural Geology in Mining and Exploration*. Geology Department and University Extension, University of Western Australia, Publ., **25** : 38-42.
- Sibson, R.H., Robert, F. and Poulsen, K.H., 1988. High-angle reverse faults, fluid-pressure cycling, and mesothermal gold-quartz deposits. *Geology*, **16**: 551-555.

Tyler, R., 1989. Cyclic sedimentation and gold mineralization in the Malmani Dolomite Sub-Group, Pilgrim's Rest-Sabie area, eastern Transvaal. Unpublished M.Sc. thesis, Univ. Witwatersrand, Johannesburg, 145pp.

Visser, N.H. and Verwoerd, W.J., 1960. The geology of the country north of Nelspruit. Explanation to Sheet 22, (Nelspruit). Geol. Surv. S. Afr., 128pp.

Von Dessaer, A., 1912. Notes on the vertical and bedded veins of Pilgrim's Rest. Trans. geol. Soc. S. Afr., 15: 146-154.

Zietsman, A.L., 1967. The relationship between mineralisation and structure in the Pilgrim's Rest-Sabie Gold-Field. Unpublished Ph.D. thesis, Univ. Orange Free State, Bloemfontein, 198pp.

_____oOo_____